High-Gain Meanderless Slot Arrays on Electrically Thick Substrates at Millimeter-Wave Frequencies

Meide Qiu, Michael Simcoe, and George V. Eleftheriades, *Member, IEEE*

***Abstract*—This paper introduces new techniques and architectures for the implementation of linear slot arrays on electrically thick dielectric substrates at millimeter-wave frequencies. The slot arrays are fed by a coplanar waveguide series line and lead to high gain by utilizing the phase cancellation technique to reduce coupling to the dominant surface-wave mode. Unlike traditional designs, no meander lines are used in the proposed structures, easing their fabrication by eliminating the need for air bridges and leading to patterns with low cross-polarization and high gain. In addition, the option of including a backing ground reflector to render the patterns unidirectional is explored and implemented. In this latter case, it is shown that simultaneous reduction of the dominant surface-wave and TEM modes through phase cancellation can be achieved. The design of the proposed arrays is based on an intuitive transmission-line model, which enables the implementation of arrays with a gradual current taper and, thus, maximum gain. This study is verified experimentally around a nominal frequency of 27.8 GHz.**

***Index Terms*—Integrated-circuit antennas, meander lines, millimeter waves, series feeding, slot arrays, surface waves, wireless links.**

I. Introduction

MILLIMETER-WAVE printed antennas can suffer from severe surface-wave losses due to the fact that standard substrates become electrically thick as the frequency increases well within the millimeter-wave spectrum. The practical implication of the strong coupling to surface waves is the scattering of this power from substrate edges, resulting in poor radiation patterns and reduced gain. Nevertheless, in many instances, high-gain patterns are very desirable in order to conserve precious millimeter-wave power in wireless links.

One way to reduce surface-wave coupling from antennas printed on electrically thick substrates is by utilizing phase cancellation techniques. An early account of this approach has been reported by Pozar [1] for the case of elementary printed dipole antenna arrays. In that paper, it was pointed out that collinear dipoles, spaced by half a guide wavelength (for the TM_0 mode) lead to phase cancellation of the surface-wave power along the collinear axis. Contemporary with that paper, similar concepts were described by Rutledge *et al.* in [2] for the case of elementary broadside twin slots. In fact, the case of slots is a more practical one because slots couple to the dominant TM_0 mode along the perpendicular direction to their axis (broadside), which can alleviate the complexity of the required feed network. Later on, Rogers and Neikirk introduced and demonstrated practical microstrip-fed structures of such half a guide wavelength spaced broadside twin-slot elements [3]–[5]. Subsequently, Laheurte *et al.* examined the twin-slot configuration, but when fed by a coplanar waveguide (CPW) line [6]. A summary of some of these results, including several examples of practical millimeter-wave antenna mixers built around the twin-slot element, can be found in [7]. More recently, the concept of utilizing phase cancellation to reduce surface-wave losses has been extended in a straightforward manner to linear arrays of half a guide wavelength spaced slot elements in [8]. In that paper, the slot arrays are series-fed by a CPW line. However, two important limitations can be identified there. The first one stems from the use of a meandered series feed line in order to excite the slots in phase while keeping the interelement distance equal to a half a guide wavelength of the dominant TM_0 surface-wave mode. One implication of this approach is that, for a given number of slots, the length of the array is reduced (compared to a corresponding array without a meander line), thus ultimately limiting the available gain *per feed-line length*. In addition, the meander line can introduce *significant* cross-polarization, as will be experimentally demonstrated in this paper, thus further reducing the antenna array gain. A solution to this problem has been proposed in [9] and [10], where it has been theorized that the slot elements can be fed with a meanderless (straight) CPW series feed line, maintaining comparable radiation efficiency and while still exciting the slots in-phase. In fact, this approach leads to linear slot arrays with higher gain for a given number of slot elements (i.e., feed-line loss). The second limitation in [8] appears to be the *strong* current taper reported along the fabricated arrays, which yielded patterns of relatively wide beamwidth and, thus, reduced gain. This strong taper also restricted the ability of gain increase by means of elongating the arrays beyond four end-fed elements [8]. In this paper, the problem of the current taper along the array is also tackled and practical guidelines are proposed and demonstrated for its minimization.

The work in [9] and [10] merely predicted the possibility of such meanderless high-gain slot arrays under the assumption of a *uniform* current excitation. In this regard, neither a particular feed mechanism and its effects on the array have been described, nor any dedicated design procedure has been specified. Indeed, as will be shown in this paper, the specific feed mechanism and the associated current taper, stemming from conductor and mismatch losses, have to be seriously considered for the successful design of the proposed meanderless arrays at millimeter-wave frequencies. It will be demonstrated that, with a proper design of the arrays, an almost uniform current distribution can be achieved for reasonably long arrays. The purpose of

Manuscript received September 13, 2000.

The authors are with the Edward S. Rogers Sr. Department of Electrical and Computer Engineering, University of Toronto, Toronto, ON, Canada M5S 3G4.

Publisher Item Identifier S 0018-9480(02)01164-X.

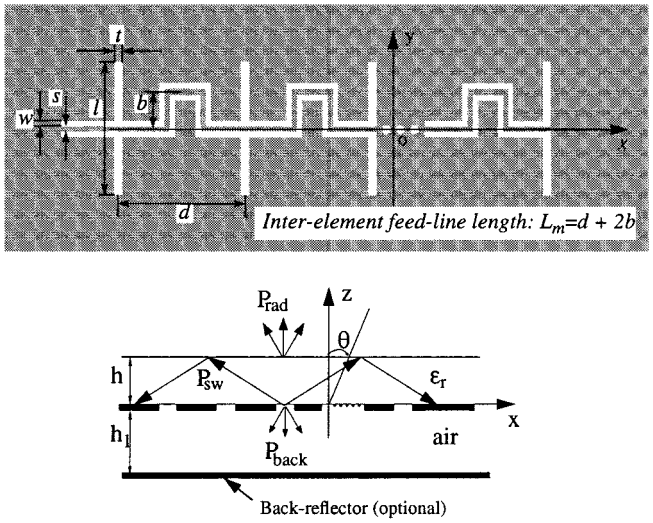

Fig. 1. Geometry of a CPW series-fed slot array.

this paper is to introduce the design, analysis, implementation, and testing of practical meanderless high-gain CPW-fed slot arrays. This extends to the important issue of backing these slot arrays with a ground reflector in order to render their patterns unidirectional and further increase their gain [11].

This paper is organized as follows. In Section II, the basic concepts and principle of operation of the proposed arrays are outlined. Section III is devoted to the introduction of a design strategy that leads to a *gradual* current taper along the array and a matched voltage standing-wave ratio (VSWR) at its feed point. The design is based on a handy transmission line (TL) model and full-wave HP Momentum simulations. Section IV describes supporting numerical and experimental results, which include a comparison with a standard meander-line fed slot array, absolute gain measurements, and a corresponding detailed loss budget breakdown for the proposed arrays. The experimental results extend to the characterization of conductor-backed unidirectional arrays of the same kind.

II. Theory

The geometry of the CPW series-fed linear slot arrays considered in this paper is shown in Fig. 1. For generality, the feed line is shown meandered. Also, the array of Fig. 1 is shown as end fed, but it should be understood that, in general, the array may be fed from its center (center fed) as well. The center feeding is useful for doubling the length (directivity) of an array for a given current taper on each arm. Finally, the option of utilizing a back reflector at the back side (air side) of the array to render the patterns unidirectional is also included. Such an antenna array will have a radiation efficiency defined by (see Fig. 1)

$$\eta = P_{\rm rad}/(P_{\rm rad} + P_{\rm sw} + P_{\rm back}) \tag{1}$$

where $P_{\rm rad}$ represents the useful radiated power through the substrate, $P_{\rm back}$ is the power leaking from the back side of the substrate, and $P_{\rm sw}$ represents the total power coupled to surface-wave modes. It should be noted that material losses $P_{\rm mat}$ that account for conductor and dielectric losses should also be included in the efficiency calculations. However, this is not done explicitly in the definition of (1) in order to facilitate the subsequent discussion of the feed-line effects, as will become obvious later on. This efficiency defines a corresponding antenna gain given by the usual expression

$$G = \eta D \tag{2}$$

where D is the array directivity. In order to specifically examine the power leakage from the back (air) side of the array, the radiation efficiency of (1) can be factorized as $\eta = \eta_{\rm sw}\eta_{\rm back}$, where

$$\eta_{\rm sw} = (P_{\rm rad} + P_{\rm back})/(P_{\rm rad} + P_{\rm sw} + P_{\rm back}) \tag{3}$$

is the surface-wave suppression efficiency and

$$\eta_{\rm back} = P_{\rm rad}/(P_{\rm rad} + P_{\rm back}) \tag{4}$$

is the back radiation suppression efficiency. In the case that a back reflector is present, $P_{\rm back}$ is identical to the power coupled to the TEM, which can now propagate between the slot and reflector ground planes.

In this paper, only quarter-dielectric-wavelength-thick substrates are considered, which lead to maximum front-to-back ratio of the radiated power density at broadside [3]. Furthermore, without loss of generality, the substrate relative permittivity is assumed $\epsilon_r = 4.5$, which corresponds to a Rogers TMM4 substrate used for the experimental part of this study. The excited surface-wave modes are in reality cylindrical waves, which require two indexes for their classification. However, as was clarified in [10], familiar single-index transverse magnetic TM_m and transverse electric TE_m surface-wave modes can be introduced, which do not exhibit any azimuthal variation. Instead, the azimuthal dependence of each one of these modes is now contained in a surface-wave pattern over the substrate [10]. For example, the longitudinal z-component (perpendicular to the substrate) far-field substrate electric field for the TM_m mode, generated by a magnetic current (M_x, M_y), can be written in cylindrical (ρ, ϕ, z) coordinates as

$$E^{ff}_{sw,\,z}(\overline{\rho}) = A_{m1} f^{TM}_m(z) \sqrt{\frac{2j}{\pi\beta\rho}}\, e^{-j\beta\rho} \sum_{n=-\infty}^{\infty} j^n C_n(\beta) e^{-jn\phi} \tag{5}$$

with

$$f^{TM}_m(z) = \begin{cases} \dfrac{\beta}{jk_c}\cos(k_c z), & 0 \le z \le h \\ \dfrac{\beta}{jq}\sin(k_c h) e^{-q(z-h)}, & z > h \end{cases} \tag{6}$$

and

$$\begin{aligned} C_n(\beta) = {} & \int M_x(\rho', \phi') \frac{j}{2} \Big[J_{n-1}(\beta\rho') e^{j(n-1)\phi'} \\ & + J_{n+1}(\beta\rho') e^{j(n+1)\phi'} \Big]\, ds' \\ & - \int M_y(\rho', \phi') \frac{1}{2} \Big[J_{n-1}(\beta\rho') e^{j(n-1)\phi'} \\ & - J_{n+1}(\beta\rho') e^{j(n+1)\phi'} \Big]\, ds' \end{aligned} \tag{7}$$

where the superscript ff represents far-field quantities, k_c and q are the longitudinal wavenumbers in the dielectric and air regions, respectively, β is the modal propagation constant, A_{m1} is the modal coupling constant, and $J_n(x)$ is the Bessel function of the first kind of order n. The azimuthal substrate surface-wave pattern for the TM_m mode can be identified with the summation in the right-hand side of (5). With the above definitions, the problem considered here is how to choose the inter-element distance d in Fig. 1 so that an optimum gain G is achieved for a given number of slots (i.e., series feed-line length). As was previously mentioned, the surface-wave power coupled to the dominant TM_0 mode is to be reduced by means of phase cancellation. For maximum gain, the slot currents should be excited in-phase and with equal magnitude. However, for all practical cases, this condition of uniform currents can never be satisfied due to material and mismatch losses on the series feed line. In this regard, the feed line introduces a current taper along the array, which has to be accounted for in the design of high-gain slot arrays at millimeter-wave frequencies. The problem of calculating the radiation efficiency and the corresponding gain from an arbitrary slot type magnetic current distribution, including the case of linear slot arrays, has been solved in a comprehensive way in [9] and [10], and here, only the relevant results are shown and discussed.

Consider the case of a uniformly excited linear array with the nominal inter-element distance $d = 0.5\lambda_g$, where λ_g is the wavelength of the dominant TM_0 mode. The significance of this inter-element distance lies in the fact that it corresponds to complete surface-wave cancellation along the array axis (i.e., a surface-wave pattern null). Initially, it is assumed that the array is not backed by a ground reflector. The problem of determining the minimum number of slots for achieving maximum radiation efficiency in the case of $d = 0.5\lambda_g$ has been treated in [9] and [10]. It was found that the most significant improvement in efficiency takes place when adding a second slot to the original one. Additional slot elements up to eight continue to increase the efficiency, but at a slower rate. Beyond eight slots, the efficiency improvement saturates due to the ever existing back-side radiation. One way to recover the back-side radiation is by means of a ground reflector, as implied in Fig. 1. However, in such a case, extra care should be taken in order to minimize the coupling to the TEM mode, which can now propagate between the slot and reflector ground planes. This latter point is further elaborated in the remainder of this section.

From the previous discussion, a nominal eight-slot array is adopted here, which represents the minimum number of uniformly excited elements required in order to achieve almost complete surface-wave suppression for $d = 0.5\lambda_g$. The next question to be answered is whether the inter-element distance d can be increased beyond the nominal value of a half a guide wavelength with the purpose of: 1) increasing the length of the array (for a given feed-line length) and, thus, its gain; 2) simplifying the feed network, ideally eliminating the need for a meander-line feed; and 3) minimizing the coupling to the TEM mode in case a back reflector is present. In order to answer these questions, first the efficiency and gain of the eight-slot array on the substrate without a back reflector is plotted in Fig. 2(a) as a function of the inter-element distance d for two different current distributions along the array. In all cases, it is assumed that the meander feed line is adjusted to excite the slots in phase. In addition, the slots are assumed radiating at their second res-

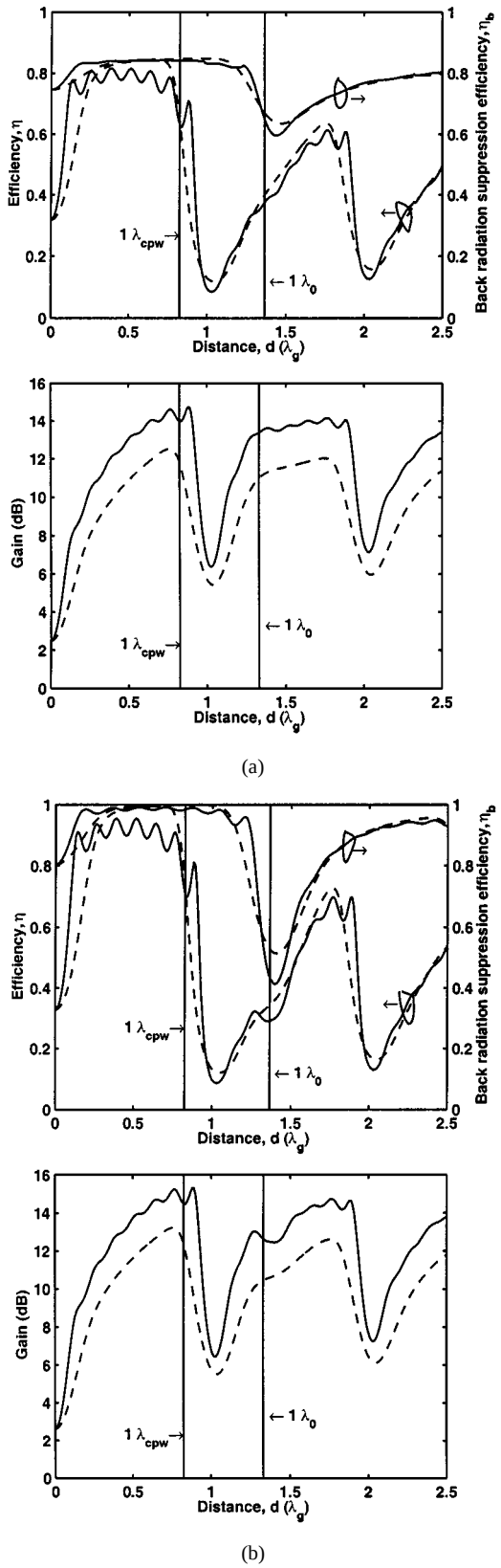

Fig. 2. Efficiency and gain of an eight-slot array printed on a substrate of $\epsilon_r = 4.5$: (a) without and (b) with a back reflector. Slot-length $l = 1.0\lambda_{\mathrm{cpw}}$, —: uniform and – – –: binomial current distribution.

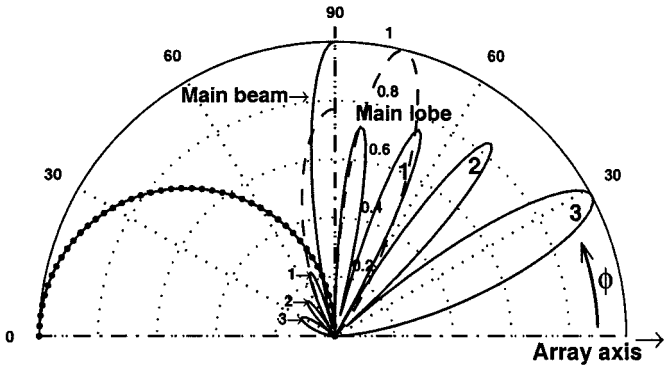

Fig. 3. Left half: surface-wave slot element field pattern (•••), uniform array factor (—), and binominal array factor (– – –). Right half: corresponding total surface-wave field patterns (multiplication of element pattern and array factor) for an eight-slot array with $d = 0.5\lambda_g$.

onance, which leads to a higher radiation efficiency compared to first resonance [10]. The chosen current distributions correspond to the two extremes of uniform and binomial slot current excitations. It should be pointed out that the binomial distribution is symmetric and would require center feeding for its realization. Also, the material losses $P_{\rm mat}$ are not directly accounted for because, in all cases, the series feed-line length and, thus, these losses, remain constant. As shown in Fig. 2(a), for both distributions, maximum radiation efficiency takes place when the inter-element distance is close to a half a guide wavelength $d = 0.5\lambda_g$. However, as Fig. 2(a) also demonstrates, this choice does not lead to the highest possible gain. In fact, a much more desirable position corresponds to an inter-element distance of one CPW feed-line wavelength, which is about equal to one mean wavelength, i.e., $d = \lambda_{\rm cpw} \approx \lambda_0/\sqrt{\epsilon_m}$, $\epsilon_m = (\epsilon_r+1)/2$. Indeed, for the considered eight-slot array, this choice leads to a longer antenna and, hence, a higher gain equal to 14.0 dB, while *no meandering* of the feed-line is necessary [see Fig. 2(a)]. The corresponding gain for a meandered feed-line is 13.0 dB for the $d = 0.5\lambda_g$ case. As will be demonstrated in the following section, in practice, the presence of the meandered feed line produces excessive cross-polarization, which further degrades the achievable gain beyond what Fig. 2(a) predicts.

The case of including a back reflector at a distance $h_1 = \lambda_0/4$ (see Fig. 1) away from the slot ground plane is treated in Fig. 2(b), which shows the radiation efficiency and gain as a function of the inter-element distance d. As shown in Fig. 2(b), in comparison to Fig. 2(a). within the region of interest $0.5\lambda_g \leq d \leq \lambda_{\rm cpw}$, the back reflector is very effective in increasing the overall radiation efficiency through the reduction of the back radiation loss. This implies that within this inter-element distance range, the array results in a *simultaneous* phase cancellation of the dominant surface wave and the TEM parallel-plate modes [11]. Once more, maximum gain corresponds to the uniform current distribution as Fig. 2(b) implies.

An interesting observation that can be made from Fig. 2 is that the binomial current taper around $d = 0.5\lambda_g$ results in an overall higher efficiency than the uniform one. This rather counter-intuitive observation can be explained by examining the normalized surface-wave patterns for the dominant $\rm TM_0$ mode in the two cases. This is done in Fig. 3, which shows the surface-wave pattern array factors for the uniform and binomial distributions, as well as the single-slot element pattern (left half), and the corresponding overall surface-wave patterns (right half). As shown, for the case of the uniform current distribution, the surface-wave power is contained in 16 lobes (only four lobes are shown in Fig. 3), which correspond to the four main lobes and the 12 sidelobes of the array factor. On the other hand, the surface-wave array factor for the binomial distribution exhibits *no sidelobes* and the only contribution to the corresponding surface-wave pattern arises from its main lobes, thus leading to a higher radiation efficiency, as implied by Fig. 3. Although this is an interesting result, as Fig. 2(b) shows, for equal length arrays, the uniform current distribution still results in a higher gain than the binomial current distribution.

TABLE I
EFFICIENCY AND GAIN FOR AN EIGHT-SLOT ARRAY ON A SUBSTRATE OF $\epsilon_r = 4.5$, $h = \lambda_d/4$ WITH AND WITHOUT A BACK REFLECTOR

		Without a back-reflector		With a back-reflector	
	Current distribution	$d = 0.5\lambda_g$	$d = 1.0\lambda_{cpw}$	$d = 0.5\lambda_g$	$d = 1.0\lambda_{cpw}$
Efficiency (%)	uniform	81.1	63.5	94.7	71.2
	binomial	83.8	65.3	99.0	73.8
Gain (dB)	uniform	13.0	14.0	13.7	14.5
	binomial	10.9	11.9	11.6	12.4

Table I summarizes the performance of eight-slot arrays with inter-element distances of $d = 0.5\lambda_g$ and $d = 1.0\lambda_{\rm cpw}$ for uniform and binomial distributions, with and without a back reflector. As can be inferred from Table I, the meanderless choice ($d = 1.0\lambda_{\rm cpw}$) with uniform current excitation and a back reflector leads to the highest gain of 14.5 dB. It should be pointed out that, in addition to the analysis of Table I, this inter-element distance simplifies the fabrication process and does not induce any appreciable cross-polarization, in contrast to the nominal case of $d = 0.5\lambda_g$ that would require a meandered feed line.

As mentioned previously, for the case of $d = 0.5\lambda_g$, an array with eight slots approaches its maximum efficiency [9], [10]. On the other hand, for the meanderless case of $d = 1.0\lambda_{\rm cpw}$, the efficiency can be further increased by the addition of more slots, as shown in Fig. 4. Indeed, as Fig. 4 indicates, both the radiation efficiency and antenna gain increase with the number of slots. As an example, Fig. 5 shows the radiation efficiency and gain of a 16-slot array with a back reflector as a function of the inter-element distance d. Compared to the case of the eight-slot array [see Fig. 2(b)], it is clear that the 16-slot array characteristics vary more smoothly with d and that, at the meanderless position $d = 1.0\lambda_{\rm cpw}$, a higher efficiency and gain are achieved. Table II compares the performance of a 16-slot array with inter-element distances of $d = 0.5\lambda_g$ and $d = 1.0\lambda_{\rm cpw}$ for a uniform current distribution with and without a back reflector. It is observed that the meanderless line (straight) fed 16-slot array leads to about 2 dB higher gain than the meander-line fed one without any appreciable sacrifice to the antenna radiation efficiency.

An apparent disadvantage of the chosen distance $d = 1.0\lambda_{\rm cpw}$ is the possible limited gain bandwidth implied by Fig. 2. Nevertheless, this is not a real limitation because, in any case, the series feed mechanism results in a narrow-band VSWR input impedance match and an associated

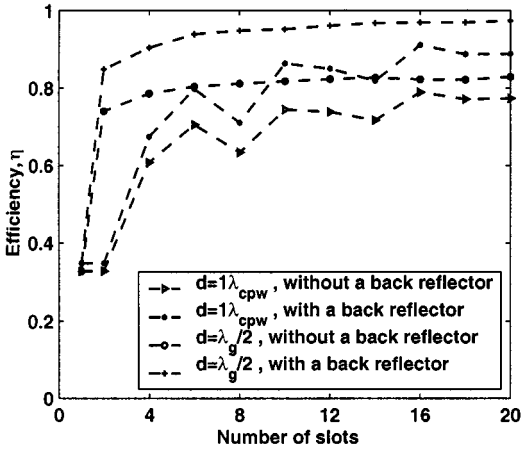

(a)

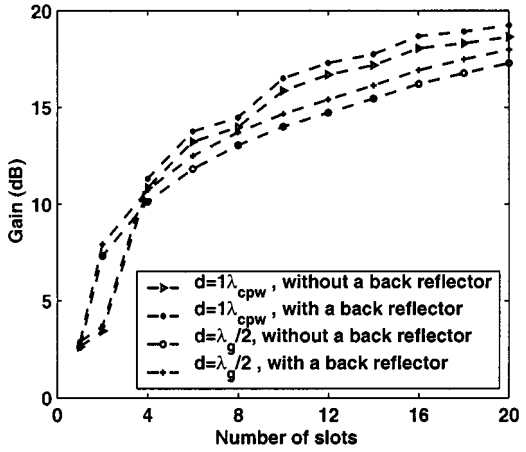

(b)

Fig. 4. (a) Efficiency and (b) gain versus the number of slots with uniform current distribution ($\epsilon_r = 4.5, h = \lambda_d/4$).

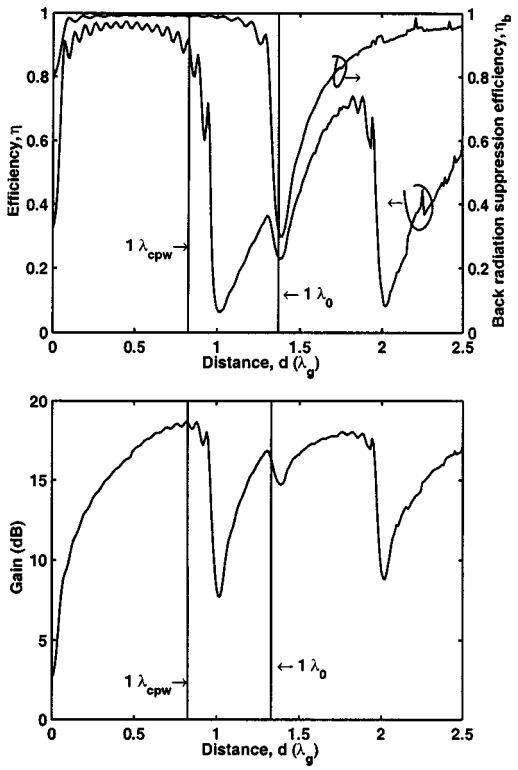

Fig. 5. Efficiency and gain of a 16-slot array printed on a substrate of $\epsilon_r = 4.5, h = \lambda_d/4$ and with a back reflector. Slot-length $l = 1.0\lambda_{\rm cpw}$ (uniform excitation).

TABLE II
EFFICIENCY AND GAIN FOR A UNIFORM 16-SLOT ARRAY ON A SUBSTRATE OF $\epsilon_r = 4.5, h = \lambda_d/4$ WITH AND WITHOUT A BACK-REFLECTOR

	Without a back-reflector		With a back-reflector	
	$d = 0.5\lambda_g$	$d = 1.0\lambda_{cpw}$	$d = 0.5\lambda_g$	$d = 1.0\lambda_{cpw}$
Efficiency (%)	82.2	78.9	96.9	91.1
Gain (dB)	16.2	18.1	16.9	18.7

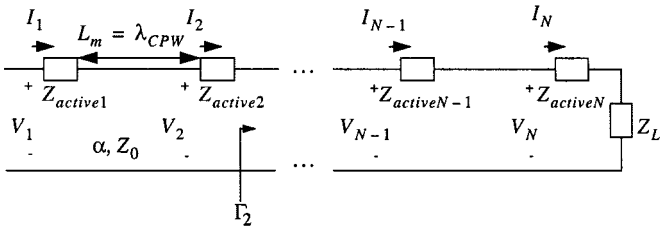

Fig. 6. TL model for the series-fed slot array.

beam squint with frequency, naturally limiting the bandwidth within a range of about 3%. The issue of the robustness of the proposed arrays with frequency variation is further examined experimentally and numerically in Section IV.

III. DESIGN PROCEDURE

The CPW-fed slot array can be associated with the dual of a two-wire fed dipole array. It is well known that such a dipole array can be represented by shunt impedances loading the feed TL [12]. Based on this fact and duality considerations, the CPW-fed linear slot array can be modeled as a TL network with the slots appearing as series impedances, as shown in Fig. 6. In order to account for mutual coupling effects, each slot should be represented by its active input impedance defined by

$$Z_{m,\,\text{active}} = \frac{V_m}{I_m} = \sum_{i=1}^{N} Z_{mi}\,\frac{I_i}{I_m}, \qquad m = 1, 2, 3, \ldots, N \tag{8}$$

where Z_{mm} represents the self impedance of a slot and Z_{mi} ($m \neq i$) represents the mutual impedance between a pair of slots. The slots in the array are designed to operate at their second resonance in order to achieve wider VSWR bandwidth [13] and minimize coupling to the dominant surface-wave mode [10]. Another important benefit of utilizing full-wavelength slots will be revealed later.

A very important consideration for the design of these arrays is the effect of conductor and reflection losses along the axis of the array. At millimeter-wave frequencies, the feed-line losses can be significant and combined with a possible impedance mismatch can produce a strong taper in the current distribution along the array, which, in turn, would reduce the achievable gain. Based on the simple TL model of Fig. 6, a parametric study

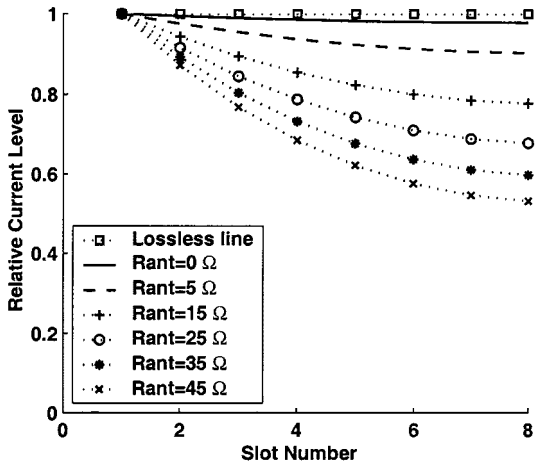

(a)

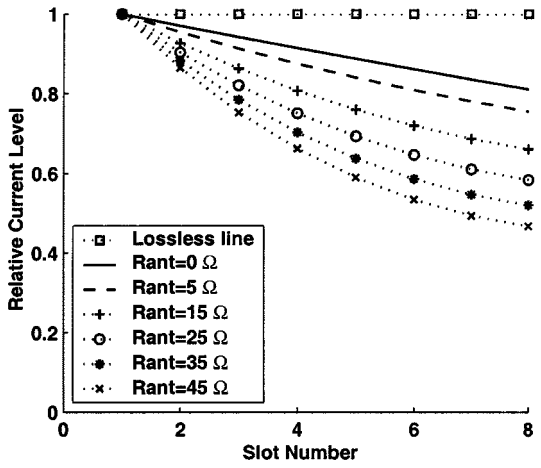

(b)

Fig. 7. Relative slot current distribution for an end-fed eight-slot array with a feed line of $Z_0 = 50\ \Omega$, $\alpha = 0.03Np/\lambda_{\rm cpw}$ terminated to: (a) a short and (b) matched load ($d = L_m = 1.0\lambda_{\rm cpw}$).

of the taper influencing variables has been undertaken and representative results for an eight-slot array are shown in Fig. 7(a) and (b) for a short and a 50-Ω termination, respectively (with a feed-line characteristic impedance of 50 Ω). These figures display the relative current level along the length of the array as a function of the active impedance of the slots for the lossless ($\alpha = 0$) and the experimentally achieved ($\alpha = 0.03Np/\lambda_{\rm cpw}$) case, as will be described in the following section. In addition, the active slot input impedances are assumed real and equal ($Z_{m,\,\rm active} = R_{\rm ant}$, $m = 1, 2, \ldots, 8$), a condition that can be closely achieved in practice, as will be shown below.

First, note from Fig. 7 that, for the lossless case, there is *no taper* in the current distribution. This is expected since, in this case, $L_m = 1.0\lambda_{\rm cpw}$ (see Fig. 1) and the slots are separated by one CPW wavelength; thus, all appearing in series at the input of the feed line. It should be noted that this conclusion uncovers an oversight in [8], which analyzes such arrays as traveling wave ones; thus, implying that even when the slots are separated by one CPW wavelength, the lossless case would still result in a current taper along the array (set $\delta = 1$ in [8, eq. (6)]). On the other hand, the situation dramatically changes when there is finite loss on the CPW feed line. Indeed, as can be observed from Fig. 7, for a given loss factor per section, i.e., α, the current taper is *highly* dependent upon the active resistance per slot $R_{\rm ant}$. As indicated, the smaller the slot resistance, the more gradual the taper along the line. Related to this is the interesting conclusion that can be drawn when comparing Fig. 7(a) and (b), namely, for a given $R_{\rm ant}$, a 50-Ω termination leads to a stronger taper than a short-circuit termination. A simple explanation for these observations can be obtained by considering the TL equivalent circuit of Fig. 6, which implies that the ratio between the currents of the $n^{\rm th}+1$ and $n^{\rm th}$ slots is simply given by

$$\frac{I_{n+1}}{I_n} = e^{-\alpha}\,\frac{1-\Gamma_{n+1}}{1-e^{-2\alpha}\Gamma_{n+1}} \tag{9}$$

where Γ_{n+1} is the reflection coefficient when looking down the line from the $n^{\rm th}+1$ slot (see Fig. 6). As (9) implies, when the reflection coefficient Γ_{n+1} vanishes, the taper simply becomes equal to $e^{-\alpha}$, corresponding to a matched lossy line. However, (9) also implies that an even *more gradual* taper (i.e., $I_{n+1}/I_n > e^{-\alpha}$) can be achieved when Γ_{n+1} approaches the value of -1, i.e., a short circuit condition. This is not surprising since, for a short-circuit termination, the reflected current wave *adds in-phase* to the incident one, thus reducing the overall current taper along the feed line. Therefore, *as a rule of thumb, in order to minimize the current taper along the array, the slot active resistances should be kept as small as possible when contrasted to the characteristic impedance of the feed line and the line should be terminated to a short.*

Based on the previous analysis, the design goals can be summarized as follows.

1) Achieve real slot active impedances (i.e., resonance).
2) Obtain a real input impedance at the feed point (to be matched by means of a matching network, if necessary).
3) Minimize the slot active resistances in order to reduce the taper along the array.

Assuming that the inter-element distance d between slots is fixed from the gain considerations outlined in Section II, all of the above design constraints have to be accommodated by adjusting the length l and width t of each slot (see Fig. 1). The design process follows the spirit of the one presented by Elliot [12] for a series-fed dipole array and modified in [14] for the case of a series CPW-fed slot array printed on a thin dielectric substrate. However, compared to the process described in [14], the substrate here is electrically thick and Booker's relation cannot be invoked to simplify the design; instead, full-wave analysis such as HP Momentum should be utilized to generate the required self- and mutual-impedance data for all slots. Exactly following the procedure of [12] or [14] proves quite time consuming due to the excessive number of full-wave analysis iterations necessary. To this end, in order to simplify the design and minimize the amount of time-consuming HP Momentum simulations, the active input impedance data have been generated based only on the full-wave analysis of the central element in the array that closely resembles an embedded element in an infinite periodic linear array. To accomplish this, first for a given slot width t, the isolated slot input impedance (real and imaginary parts) is generated as a function of the slot length l using HP Momentum. In this way,

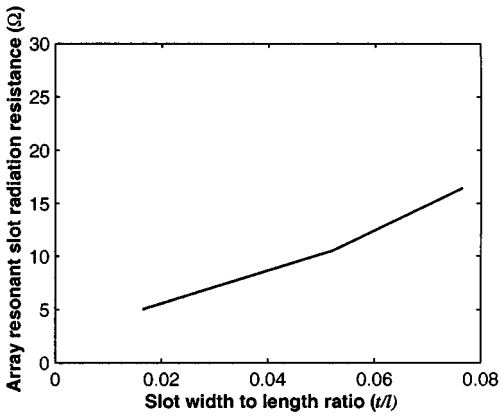

Fig. 8. Active slot radiation resistance at second resonance versus slot width-to-length ratio ($d = \lambda_{\rm cpw}$, $\epsilon_r = 4.5$, $h = \lambda_d/4$).

the isolated slot resonant length can be identified. Afterwards, the corresponding driving point impedance of the entire array is obtained, also based on HP Momentum full-wave simulations. From the TL model of Fig. 6 and since the slots are separated by $1.0\lambda_{\rm cpw}$–long feed lines, the array input impedance is the summation of all the slot active impedances. Hence, in order to obtain the (average) active impedance per slot, the array input impedance is divided through by the number of slots N. In this manner, the average slot active input impedance is directly obtained without the need to generate separate mutual impedance data for all slots. Subsequently, the slot length l is adjusted again, based on the isolated slot impedance data, in order to tune out any reactive component of the so calculated (average) active slot impedance. The process is repeated until a real active slot impedance is achieved. It was found that this technique converges after only two or three iterations, thus considerably simplifying the design procedure. Evidently, there are some inherent approximations to this approach, which become more accurate as the length of the array increases. First, not accounted for are array edge effects, and this is especially true of the last slot, which is terminated in a reactive short (although this reactance can be eliminated by extending the short beyond the final slot edge into a stub and adjusting its length [14]). Second, in reality, the equal length slots in the array may not individually achieve a pure real active slot impedance (i.e., resonance), but may have some residual reactance. Therefore, the so obtained active resistance per slot, only represents an average value across the array, which, however, proves to be a very reliable approximation for the design of the proposed meanderless slot arrays. Third, the procedure only works at the design frequency for which the slots are separated by $1.0\lambda_{\rm cpw}$-long feed lines, which is, however, adequate for design purposes. Based on this iterative design procedure, shown in Fig. 8 is the calculated active slot input resistance at second resonance as a function of the width to length ratio t/l for a slot separation $d \approx \lambda_{\rm cpw} = 6.45$ mm on a substrate of $\epsilon_r = 4.5$ and a thickness of $h = \lambda_d/4 = 1.27$ mm. First of all, it should be pointed out that, at their second resonance, slots exhibit low radiation resistance in contrast to their first resonance [13] and this is another important reason for choosing full wavelength slots. As can be seen from Fig. 8, the input resistance increases with an increased width-to-length ratio. Thus, in order to keep the slot resistance low and thereby the current taper gradual, the width-to-length ratio should be kept small.

TABLE III
CURRENT TAPER ALONG THE EIGHT-SLOT ARRAY

Slot number m	Approximate technique $\lvert I_m\rvert$	Full-wave analysis $\lvert I_m\rvert$
1	1.0000	1.000
2	0.9731	0.9771
3	0.9503	0.9577
4	0.9315	0.9407
5	0.9166	0.9273
6	0.9056	0.9173
7	0.8985	0.9096
8	0.8951	0.9053

The final result of the above design procedure for an eight-slot array at 27.8 GHz with a slot separation $d \approx \lambda_{\rm cpw} = 6.45$ mm (see Fig. 1) on a substrate of $\epsilon_r = 4.5$ and thickness $h = 1.27$ mm (no back reflector) can be summarized as follows. Slot length $l = 7.1$ mm, slot width $t = 0.12$ mm yielding a slot active input impedance of about $R_{\rm ant} = 50\ \Omega$, CPW signal width $s = 0.65$ mm, and gapwidth $w = 0.1$ mm yielding a characteristic impedance $Z_0 = 50\ \Omega$. For this CPW line configuration, the measured TL loss per section is $\alpha = 0.03Np/\lambda_{\rm cpw}$ and, therefore, for the eight-slot array, the current taper corresponds to Fig. 7(a) with $R_{\rm ant} = 5\ \Omega$. As shown, this taper is very gradual with $I_8/I_1 = 0.9$ and, thus, the array is practically uniformly excited, as will be verified experimentally in the following section. It should be pointed out here that this conclusion is in sharp contrast to the current distribution reported in [8], which exhibited a strong taper along the array mainly due to impedance mismatch effects, which were amplified by the higher conductor losses at their operating frequency of 94 GHz. One important implication to be recognized here is that, by keeping the current taper gradual, longer arrays can be built, accompanied with an actual increase of their gain. On the other hand, the accuracy of the proposed design procedure can be demonstrated by comparing the approximate current distribution along the array to the one obtained using full-wave analysis, as shown in Table III.

IV. EXPERIMENTAL AND NUMERICAL RESULTS

Based on the design described in the previous section, a series-fed eight-slot linear array has been fabricated on a Rogers TMM4 substrate with nominal parameters $\epsilon_r = 4.5$ and $h = 1.27$ mm ($h = \lambda_d/4$) at the design frequency of 27.8 GHz, as shown in Fig. 9. As was previously explained, the inter-element distance d is chosen to be $d = \lambda_{\rm cpw} = 6.45$ mm, which leads to a meanderless feed structure with in-phase slot excitation and high gain. The CPW feed line is terminated to a short and fed by a coaxial cable through a flange mounted K-connector.

The return loss of the antenna was measured with an Anritsu 360B broad-band vector network analyzer. Fig. 10 shows the measured return loss against the one simulated with HP Momentum. As shown, the resonant frequency shifts downwards by 0.5 GHz (1.8%) from the design frequency of 27.8 GHz. In order to clarify this down shift, the dielectric constant of the substrate

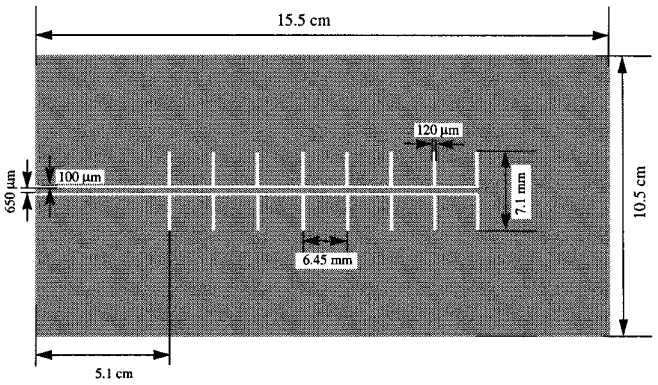

Fig. 9. Layout of the designed meanderless eight-slot antenna array at 27.8 GHz ($\epsilon_r = 4.5$, $h = 1.27$ mm).

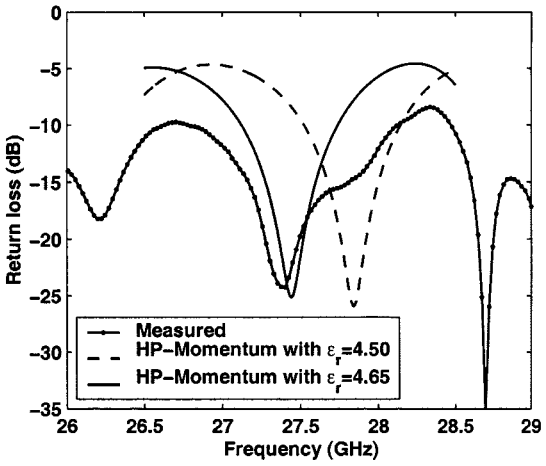

Fig. 10. Return loss of the designed meanderless eight-slot antenna array.

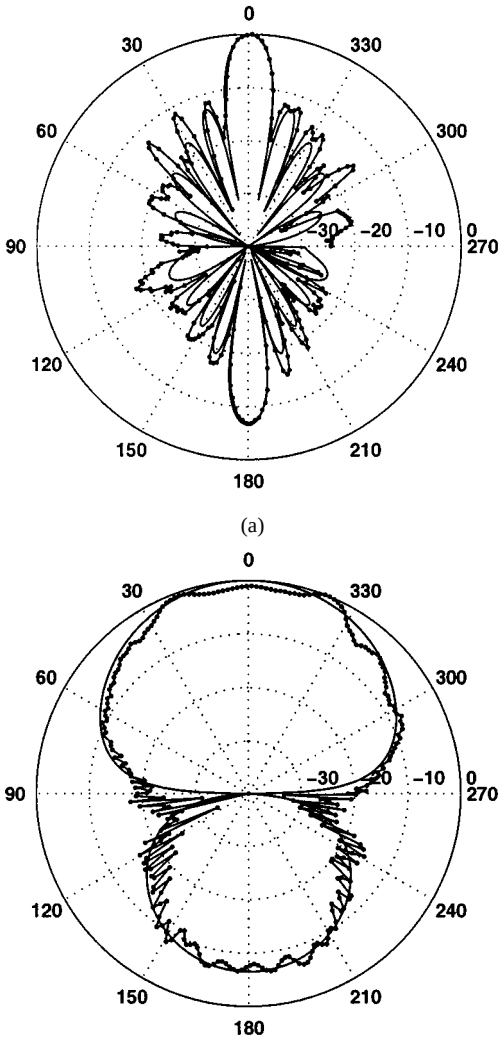

Fig. 11. Radiation patterns of the designed meanderless eight-slot antenna array at 27.8 GHz. •••: measured co-polarization; —: TL-model co-polarization. (a) E-plane. (b) H-plane.

was measured based on a gap coupled microstrip ring resonator. It was found that, around 28 GHz, the actual dielectric constant of the substrate is 4.65 instead of the nominal 4.5. When the right dielectric constant of 4.65 is used, the experimental result is in good agreement with the simulation, as shown in Fig. 10. As Fig. 10 suggests, the measured -10-dB impedance bandwidth is 1.1 GHz, which is wider than the simulated one, probably due to the effect of conductor losses, which cannot be accounted for by HP Momentum. The radiation patterns of the slot array have been measured in the anechoic chamber of the University of Toronto, Toronto, ON, Canada, having a usable size of 6.5 m $\times$ 3.5 m $\times$ 3.0 m. The slot array under test and the transmitting standard gain horn have been separated by a distance of 5 m. The test antenna resided on a rotating pedestal controlled by an Orbit AL-4802-3A positioner. A dedicated Wiltron 360B vector network analyzer has been used for the pattern measurements. The patterns at the design frequency of 27.8 GHz are compared to those obtained from the TL model of the previous section in Fig. 11. As indicated, the measured patterns are in good agreement with those predicted by the TL model of Fig. 6, especially around the broadside direction. Some discrepancies around the directions parallel to the substrate are to be expected due to the finite dimensions of the substrate. Nevertheless, the important features observed in Fig. 11 are that the patterns are smooth, which suggests that there is no appreciable degradation due to surface-wave scattering from the substrate edges. In addition, the cross-polarization level was also measured and was found to be less than -20 dB in all directions. Another important point is that the measured patterns correspond well to the patterns predicted by the TL model with the relative current excitations of Fig. 7 ($R_{\rm ant} = 5\ \Omega$), which confirms the realization of a *fairly uniformly excited slot array*. Indeed, the measured E-plane 3-dB beamwidth is 10.5°, which is very close to the 10.6° expected from a corresponding ideal eight-element uniform array. In addition, the first E-plane sidelobe level is close to the -13 dB, as expected for a uniform linear array.

The gain of the antenna was measured by the gain comparison method [15]. First, the absolute power gains of two identical horns have been measured based on the Friis transmission formula for calibration purposes. Subsequently, the gain of the designed slot array was obtained by comparison with the gain of the calibrated horn. The gain error caused by the calibration procedure, reflections at connectors, cable imperfections, and misalignment of transmit and test antennas is estimated to be about ± 0.5 dB. The highest measured gain of the antenna is

10.4 dB occurring at the input impedance resonant frequency of 27.3 GHz (see Fig. 10), which suggests that the slots are excited in-phase at 27.3 GHz. The conductor losses on the feed lines were estimated based on a through-line test board, which resulted in a measured loss of 0.4 dB/cm (which was found to be 11% higher than what HP Linecalc predicts). According to this loss value, the input feed-line loss from the K connector to the antenna input (5.1 cm, see Fig. 9) is 2.04 dB and the series feed-line loss extracted using the TL model of Fig. 6 is 1.19 dB. The conductor loss from each radiating slot is estimated from simulation to be 0.2 dB. Therefore, the deduced antenna gain at 27.3 GHz is 10.4 dB ± 0.5 dB $+2.04$ dB $+1.19$ dB $+0.2$ dB $= 13.83$ dB ± 0.5 dB, which agrees well with the theoretical prediction of 14.0 dB (see Table I).

Although the results presented thus far provide enough evidence of the validity of the proposed concept of the meanderless high-gain slot arrays and their associated design procedure, nevertheless, the rather large experimental error (± 0.5 dB) inherent to the employed gain measurement method [15] prompted further investigations. In particular, in order to make a meaningful comparison with a meander-line fed architecture at $d = 0.5\lambda_g$, a corresponding meander-line fed eight-slot array was also built and tested. This enabled a direct comparison between the different slot array designs, which eliminates the ambiguity introduced by the experimental errors, especially the error in measuring the absolute gain. For fabricating the meander-line fed slot array, the same substrate has been used and the actual feed-line dimensions remain the same as the ones of Fig. 9, in order to maintain the same feed-line conductor losses. Referring to Fig. 1, the dimensions of the fabricated meander-line fed slot array are as follows: $w = 0.1$ mm, $s = 0.65$ mm, $l = 7.16$ mm, $t = 0.12$ mm, $b = 1.2$ mm, $d = 4.275$ mm. Fig. 12 shows the measured E- and H-co- and cross-polar patterns of this antenna at the design frequency of 27.8 GHz. A striking feature of the patterns presented in Fig. 12 is the *significant cross-polarization* induced in the principal planes (-3.5 dB in the broadside direction). In addition, it becomes apparent that the quality of the patterns deteriorates when compared to those of the meanderless fed array of Fig. 11. Indeed, now the patterns develop rather distinct undulations and even the main beam at broadside is distorted. It can be theorized that both the higher cross-polarization and the reduced quality of the patterns are due to parasitic radiation from the meandered feed line. On the one hand, the meander-line directly radiates space-wave co- and cross-polarized patterns and, on the other hand, it can couple to the dominant surface-wave mode as well (probably through scattering from the meander-line bends). This distorts the patterns and increases the sidelobe level. In order to clean up the patterns and enable meaningful beamwidth, sidelobe, and gain measurements, radar absorbing material (RAM) was added to surround the substrate edges. It was observed that when RAM was added, the patterns became much smoother, but the level of cross-polarization did not decrease. Perhaps the addition of air bridges along the meandered CPW feed line could have reduced the cross-polarization level through suppression of the slot-line mode, which is probably excited. However, an attempt to do so was abandoned due to the encountered fabrication difficulty in placing air bridges in the tight space between two consecutive slots. The measured 3-dB beamwidth in the presence of the RAM was about 16°, which is larger than the corresponding 10.5° obtained for the meanderless array of Fig. 11. Of course, this is a direct consequence of the fact that this is a 33% shorter array than the corresponding meanderless one of Fig. 9. The highest measured gain (with RAM) was found to be 7.7 ± 0.5 dB, occurring at 27.3 GHz, which is about 2.7 dB lower than the gain of the straight-fed array of Fig. 9 at the same frequency. The difference between the two gains is actually 1.7 dB larger than the theoretically expected difference in gain of 1.0 dB, as predicted in Table I. The most likely reason for this discrepancy is the fact that the effect of the feed line on the cross-polarization and surface-wave levels has not been accounted for in the theory of Section II. Nevertheless, the important point which has been established here is that the performance of the meander-line fed slot array is *clearly and significantly* degraded compared to the proposed meanderless fed array of Fig. 9.

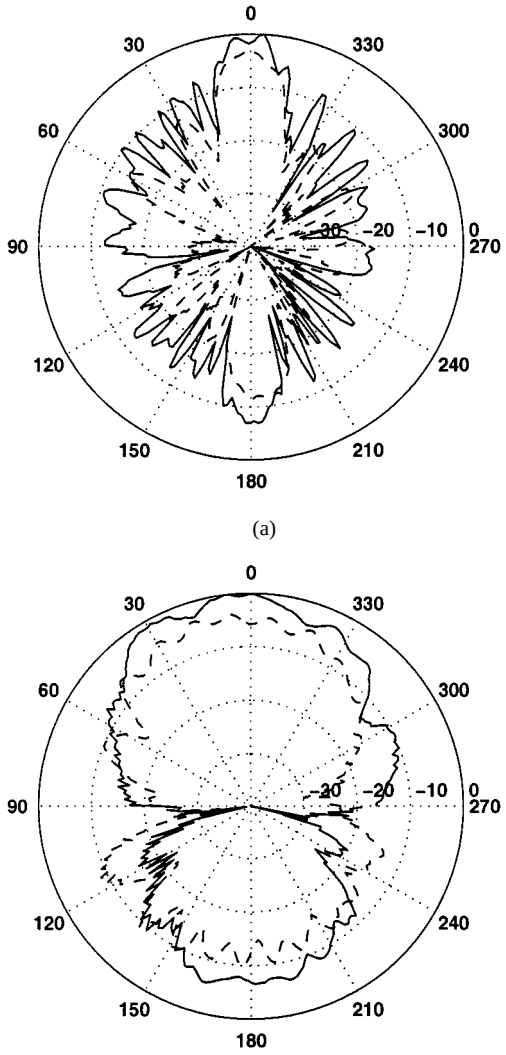

Fig. 12. Measured radiation patterns of the meandered series-fed eight-slot antenna array at 27.8 GHz. —: co-polarization, – – –: cross-polarization. (a) E-plane. (b) H-plane.

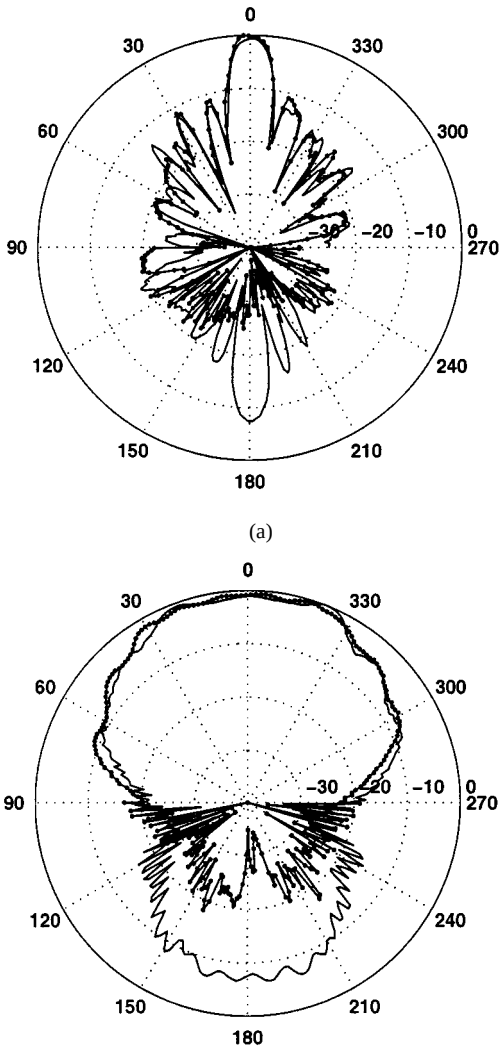

Fig. 13. Measured radiation patterns of the designed meanderless eight-slot antenna array at 27.8 GHz. •••: with a back reflector, —: without a back reflector (cross-polarization level of the array is less than -20 dB in all directions). (a) E-plane. (b) H-plane.

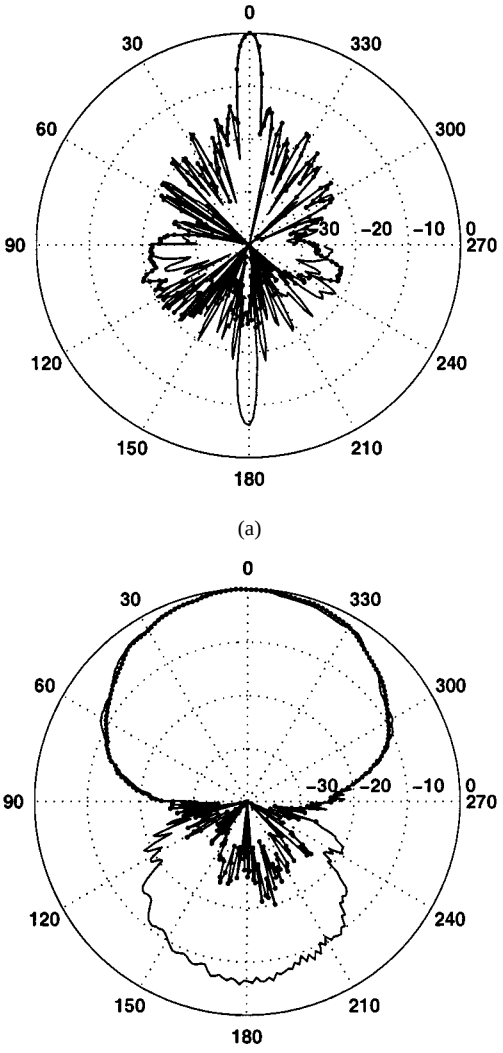

Fig. 14. Measured radiation patterns of the designed meanderless 16-slot antenna array at 27.8 GHz. •••: with a back reflector, —: without a back reflector (cross-polarization level of the array is less than -20 dB in all directions). (a) E-plane. (b) H-plane.

As mentioned in Section II, a backing ground reflector can be used to achieve unidirectional patterns and further increase the radiation efficiency. It was also predicted that, for the structure of Fig. 1, simultaneous phase cancellation of the dominant surface-wave power and the back-radiated TEM mode can be achieved. In order to verify this assertion, a backing ground reflector has been supported behind the slot/CPW ground plane of the structure presented in Fig. 9 by means of several foam posts. The distance of the back reflector from the slot/CPW ground plane was chosen to be a quarter free-space wavelength $h_1 = \lambda_0/4$ at the design frequency of 27.8 GHz in order to present an open circuit to the slots and minimize the effect on the antenna input impedance. Indeed, it was experimentally verified that, in this case, the resulting input impedance virtually does not change from the one shown in Fig. 10 (within the same frequency range). The corresponding patterns of the designed antenna array with a back reflector are compared with those without a back reflector in Fig. 13. As shown, the forward patterns remain virtually unaffected whereas the back radiation is suppressed to a level of -25 dB in the broadside direction. In addition, the cross-polarization level is not affected by the presence of the back reflector either. These observations, together with the fact that the H-plane pattern actually becomes smoother in the presence of the back reflector (see Fig. 13), suggest that the TEM mode is practically suppressed. This is confirmed by a gain measurement, which registers at 9.9 dB at 27.8 GHz. Indeed, this corresponds to a 0.5-dB gain improvement compared to the one without a back reflector, as theory predicts (see Table I).

While the eight-slot meanderless CPW-fed array has been demonstrated to be clearly superior compared to the corresponding meander-line fed array in terms of gain, pattern clarity, and cross-polarization, the meanderless array efficiency can be further improved by the addition of more slots, as was discussed in Section II (see Figs. 4 and 5). In order to demonstrate this, a meanderless 16-slot array was designed, fabricated, and tested and the same sets of measurements were performed as for the eight-slot array. The corresponding

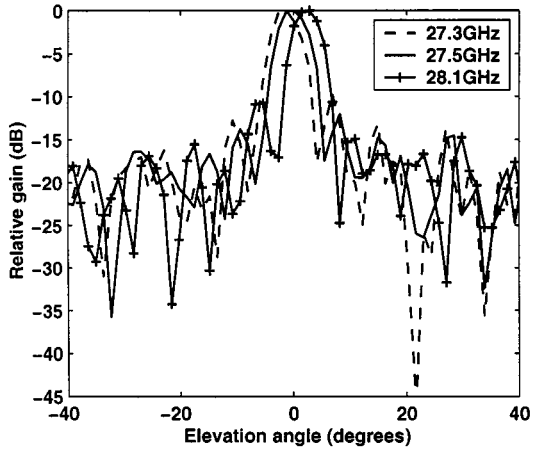

Fig. 15. Measured E-plane patterns of the designed 16-slot antenna array at different frequencies.

E- and H-plane patterns with and without a back reflector are shown in Fig. 14. As shown, the pattern parameters are still consistent with those of an approximately uniformly excited array, despite the longer feed line. This almost uniform excitation was achieved by means of the low current taper design procedure detailed in Section III. Indeed, the measured 3-dB beamwidth is 5.4°, whereas the TL-model predicts 5.3° and a uniform excitation corresponds to 5.2°. In addition, the measured sidelobe level is close to −13 dB, as with a uniform array. The pattern clarity in both the E- and H-planes is better than that of the eight-slot array (compare Figs. 13 and 14) since the surface-wave power reduction is now even more effective [see Fig. 4(a)]. As Fig. 14 also shows, the addition of a back reflector suppresses the back radiation level below −20 dB throughout the principal planes and causes no appreciable effect on the front radiation patterns or the input impedance. Furthermore, the measured cross-polarization level of the 16-slot array was small in all directions (less than −20 dB). The E-plane radiation patterns have also been measured at other frequencies, as shown in Fig. 15. As can be seen from Fig. 15, the patterns preserve their shape, sidelobe level, and beamwidth throughout the indicated frequency range of 27.3–28.1 GHz, although there is a corresponding beam squint of about 4°, which is typical for series-fed arrays. In addition, with a back reflector, it was verified that the back radiation level is restricted below −25 dB in the principal planes (at broadside) within the indicated frequency range. Furthermore, Table IV outlines the measured and theoretical gains for the reflector-backed 16-slot array at several frequencies along with a corresponding detailed loss budget calculation. As Table IV indicates, the highest measured gain has been obtained at 27.5 GHz, which implies that the slots are exactly excited in-phase at this frequency. The theoretical gains have been calculated based on this assumption and accounted for the phase shift of the slot currents with frequency. This explains why, in Table IV, the indicated theoretical gain at 27.5 GHz is higher than the gain at the design frequency of 27.8 GHz. The series feed-line losses have been calculated based upon the TL model of Fig. 6. However, in order to improve the accuracy of the calculations as the frequency varies, the actual active slot impedances have been obtained based upon (8) with self and mutual slot impedance data generated by pertinent 16-port HP Momentum full-wave simulations. As Table IV demonstrates, there is good agreement between the measured and predicted gain. Furthermore, as Table IV and Fig. 15 imply, the 16-slot array retains its main electrical characteristics within a bandwidth of about 0.8 GHz, which should be adequate for most broad-band wireless applications.

TABLE IV
GAIN BUDGET FOR THE DESIGNED MEANDERLESS 16-SLOT ARRAY AS A FUNCTION OF FREQUENCY (WITH A GROUND REFLECTOR)

Frequency (GHz)	26.9	27.5	27.8	28.1
Measured gain (dB)	13.3 ± 0.5	14.0 ± 0.5	13.2 ± 0.5	11.7 ± 0.5
Theoretical gain (dB)	17.8	18.5	18.2	17.6
Input feed-line loss (dB)	2.37	2.42	2.45	2.47
Series feed-line loss (dB)	2.48	2.05	2.50	2.61
Conductor loss on slots (dB)	0.2	0.2	0.2	0.2
Mismatch loss (dB)	0.1	0.0	0.12	0.1
Total estimated loss (dB)	5.15	4.67	5.27	5.38
Deduced gain (dB)	18.45	18.67	18.47	17.08
Difference between deduced and theoretical gains (dB)	0.65	0.17	0.27	-0.52
Experimental gain without input feed-line loss (dB)	15.67	16.42	15.65	14.17

V. CONCLUSIONS

A new high-gain meanderless CPW-series-fed linear slot array architecture, printed on electrically thick substrates, has been presented. The phase cancellation approach has been utilized to reduce coupling to the dominant surface-wave mode at millimeter-wave frequencies. This architecture offers the advantages of enabling high gain for a given feed-line length (i.e., a given feed-line loss), patterns with low cross-polarization, and ease of fabrication. Furthermore, a back reflector has been utilized to render the patterns unidirectional. In this case, it has been demonstrated that simultaneous reduction of the dominant surface-wave and TEM modes through phase cancellation can be achieved, thus further increasing the radiation efficiency and gain. In order to design the proposed arrays, a TL model has been introduced and verified, which leads to a gradual current taper along the array and, thus, high gain.

An eight-slot meanderless series-fed array and a corresponding eight-slot meander-line fed one have been fabricated and tested at 27.8 GHz for a direct comparison. The experimental results clearly demonstrated that the meanderless fed array exhibits excellent patterns in contrast to the meander-line fed one, which produces high cross-polarization, poor radiation patterns, and lower gain. In order to achieve even more effective surface-wave cancellation and simultaneously prove the attainability of gradual current taper along a larger array at millimeter-wave frequencies, a meanderless 16-slot array has also been constructed and successfully tested around 27.8 GHz. Due to the simplicity of the proposed uniplanar meanderless slot arrays, their fabrication and successful operation is scalable well within the millimeter-wave frequency spectrum.

REFERENCES

[1] D. M. Pozar, "Considerations for millimeter-wave printed antennas," *IEEE Trans. Antennas Propagat.*, vol. AP-31, pp. 740–747, Sept. 1983.

[2] D. B. Rutledge, D. P. Neikirk, and D. P. Kasilingam, "Integrated circuit antennas," in *Infrared and Millimeter Waves*, K. J. Button, Ed. New York: Academic, 1983, vol. 10, pp. 1–90.

[3] R. L. Rogers and D. P. Neikirk, "Use of broadside twin element antennas to increase efficiency on electrically thick dielectric substrates," *Int. J. Infrared Millimeter Waves*, vol. 9, no. 11, pp. 949–969, 1988.

[4] ——, "Radiation properties of slot and dipole elements on layered substrates," *Int. J. Infrared Millimeter Waves*, vol. 10, no. 6, pp. 697–728, 1989.

[5] R. L. Rogers, S. M. Wentworth, D. P. Neikirk, and T. Itoh, "A twin slot antenna on a layered substrate coupled to a microstrip line," *Int. J. Infrared Millimeter Waves*, vol. 11, no. 10, pp. 1225–1249, 1990.

[6] J. M. Laheurte, L. P. B. Katehi, and G. M. Rebeiz, "CPW-fed slot antennas on multilayer dielectric substrates," *IEEE Trans. Antennas Propagat.*, vol. 44, pp. 1102–1111, Aug. 1996.

[7] G. M. Rebeiz, "Millimeter-wave and terahertz integrated circuit antennas," *Proc. IEEE*, vol. 80, pp. 1748–1770, Nov. 1992.

[8] H. Kobayashi and Y. Yasuoka, "Slot-array antennas fed by coplanar waveguide for millimeter-wave radiation," *IEEE Trans. Microwave Theory Tech.*, vol. 46, pp. 800–805, June 1998.

[9] G. V. Eleftheriades and M. Simcoe, "Gain and efficiency of linear slot arrays on thick substrates for millimeter-wave wireless applications," in *IEEE AP-S Int. Symp. Dig.*, Orlando, FL, July 1999, pp. 2428–2431.

[10] G. V. Eleftheriades and M. Qiu, "Efficiency and gain of slot antennas and arrays on thick dielectric substrates for mm-wave applications: A unified approach," *IEEE Trans. Antennas Propagat.*, to be published.

[11] M. Qiu, M. Simcoe, and G. V. Eleftheriades, "Radiation efficiency of printed slot antennas backed by a ground reflector," in *IEEE AP-S Int. Symp. Dig.*, Salt Lake City, UT, July 2000, pp. 1612–1615.

[12] R. S. Elliot, *Antenna Theory and Design.* Englewood Cliffs, NJ: Prentice-Hall, 1981, pp. 393–397.

[13] G. V. Eleftheriades and G. M. Rebeiz, "Self and mutual admittance of slot antennas on a dielectric half-space," *Int. J. Infrared Millimeter Waves*, vol. 14, no. 10, pp. 1925–1946, Oct. 1993.

[14] T. F. Huang, S. W. Lu, and P. Hsu, "Analysis and design of coplanar waveguide-fed slot antenna array," *IEEE Trans. Antennas Propagat.*, vol. 45, pp. 1560–1565, Oct. 1999.

[15] W. H. Kummer and E. S. Gillespie, "Antenna measurements—1978," *Proc. IEEE*, vol. 66, pp. 483–507, Apr. 1978.

[16] D. M. Pozar and B. Kaufman, "Comparison of three methods for the measurement of printed antenna efficiency," *IEEE Trans. Antennas Propagat.*, vol. 36, pp. 136–139, Jan. 1988.

Meide Qiu received the B.S. and M.S. degrees in electronic engineering from the Northwestern Polytechnical University, Xi'an, China, in 1989 and 1991, respectively, the M.Eng. from the Memorial University of Newfoundland, St. John's, NF, Canada, in 1998, and is currently working toward the Ph.D. degree at the University of Toronto, Toronto, ON, Canada.

From 1991 to 1996, he was an RF and Antenna Engineer with the Shenyang Aircraft Research Institute, Shenyang, China. His current research interests include planar millimeter-wave antennas and circuits for broad-band telecommunications.

Mr. Qiu was the recipient of a 1992 URSI Young Scientist Award.

Michael Simcoe received the B.S. degree in electrical and computer engineering from the University of Toronto, Toronto, ON, Canada in 1998, and is currently working toward the M.A.Sc. degree at the University of Toronto.

His research interests include planar millimeter-wave antennas and circuits for broad-band wireless communications.

George V. Eleftheriades (S'86–M'88) received the Ph.D. and M.S.E.E. degrees in electrical engineering from The University of Michigan at Ann Arbor, in 1993 and 1989, respectively, and the Diploma in electrical engineering from the National Technical University of Athens, Athens, Greece, in 1988.

From 1994 to 1997, he was with the Swiss Federal Institute of Technology, Lausanne, Switzerland, where he was engaged in the design of millimeter-wave and sub-millimeter-wave receivers and in the creation of fast computer-aided design (CAD) tools for planar packaged microwave circuits. In 1997, he joined the Department of Electrical and Computer Engineering, University of Toronto, Toronto, ON, Canada, where he is currently an Assistant Professor. He has authored or co-authored over 50 papers in refereed journals and conference proceedings. His current research interests include millimeter-wave integrated-circuit antennas and components for broad-band wireless communications, low-loss micromachined components for $K a$-band satellite communications and local multipoint distribution services (LMDSs), submillimeter-wave receivers for remote sensing, and electromagnetic design for high-speed digital circuits.

Dr. Eleftheriades was a corecipient of the 1990 Best Paper Award presented at the 6th International Symposium on Antennas (JINA), a recipient of a 1992 Student Paper Award presented at the 1992 IEEE Antennas and Propagation Symposium, and the 1991 Distinguished Achievement Award presented by The University of Michigan at Ann Arbor. In August 2000, one of his students won First Prize in the student competition of the Symposium on "Antenna Technology and Applied Electromagnetics" (ANTEM), Winnipeg, MB, Canada.